Supplementary Material for "Surface loss simulations of superconducting coplanar waveguide resonators"

J. Wenner,[1] R. Barends,[1] R. C. Bialczak,[1] Yu Chen,[1] J. Kelly,[1] Erik Lucero,[1] Matteo Mariantoni,[1] A. Megrant,[1] P. J. J. O'Malley,[1] D. Sank,[1] A. Vainsencher,[1] H. Wang,[1,2] T. C. White,[1] Y. Yin,[1] J. Zhao,[1] A. N. Cleland,[1] and John M. Martinis[1,a)]

[1)] *Department of Physics, University of California, Santa Barbara, CA 93106, USA*

[2)] *Department of Physics, Zhejiang University, Hangzhou 310027, China*

(Dated: 5 August 2011)

Calculations are provided for the equations in the manuscript "Surface loss simulations of superconducting coplanar waveguide resonators". We provide a table of surface loss participation ratios for different geometries.

I. DERIVATION OF SURFACE LOSS MODEL

In Eq. (1) of the main manuscript, the participation ratio for interface i is given by[1,2]

$$p_i = W^{-1} t_i \epsilon_i \int ds\, |E|^2, \tag{S1}$$

where the interface has a small thickness t_i, dielectric constant ϵ_i, and length coordinate s and where the resonator structure has an energy per unit length W.

The metal-air (ma) interface consists of the metal, a thin metal oxide with thickness $t_{\rm ma} \simeq 3\,$nm and dielectric constant $\epsilon_{\rm ma}$, and the outer air (vacuum) with $\epsilon_{\rm a} = 1$. The electric field must be perpendicular to the metal surface, and because the interface layer is thin, we also approximate it as perpendicular in the dielectric, so $E_{\rm ma} = E_{\rm ma\perp}$. The continuity of ϵE at the metal-oxide and air interface requires $\epsilon_{\rm ma} E_{\rm ma\perp,t} = E_{\rm a\perp,t}$. Since the oxide is thin, E does not change significantly over the oxide thickness. Combining all these results gives $E_{\rm ma} \approx E_{\rm a\perp}/\epsilon_{\rm ma}$, so the participation ratio of the metal-air oxide is

$$\begin{aligned} p_{\rm ma} W/t_{\rm ma} &= \epsilon_{\rm ma} \int ds\ |E_{\rm ma}|^2 \\ &= \epsilon_{\rm ma} \int ds\ |E_{\rm a\perp}/\epsilon_{\rm ma}|^2 \\ &= \epsilon_{\rm ma}^{-1} \int ds\ |E_{\rm a\perp}|^2. \end{aligned} \tag{S2}$$

For the metal-substrate interface, we assume a thin dielectric layer of unknown origin between the metal and substrate, which might arise from a chemical reaction of the metal to the substrate or chemi- or physi-sorbed water on the wafer surface. As before, the electric field is perpendicular to the metal and the continuity of the displacement field requires $\epsilon_{\rm ms} E_{\rm ms\perp,t} = E_{\rm s\perp,t}$, where ms represents this dielectric and s the substrate. Thus, we find $E_{\rm ms} \approx E_{\rm s\perp}\epsilon_{\rm s}/\epsilon_{\rm ms}$, so the participation ratio of the metal-substrate layer is

$$\begin{aligned} p_{\rm ms} W/t_{\rm ms} &= \epsilon_{\rm ms} \int ds\ |E_{\rm ms}|^2 \\ &= \epsilon_{\rm ms} \int ds\ |E_{\rm s\perp}\epsilon_{\rm s}/\epsilon_{\rm ms}|^2 \\ &= (\epsilon_{\rm s}^2/\epsilon_{\rm ms}) \int ds\ |E_{\rm s\perp}|^2. \end{aligned} \tag{S3}$$

For the substrate-air interface, there can be a dielectric layer from surface water or other contaminants from the air, described by a subscript sa. In addition to the perpendicular electric field which obeys $E_{\rm sa} \approx E_{\rm a\perp}/\epsilon_{\rm sa}$ as before, there are also parallel field components obeying the boundary condition $E_{\rm a\parallel} = E_{\rm sa\parallel} = E_{\rm s\parallel}$, since the interface layer is thin. Hence, the participation ratio of the substrate-air interface layer is

$$\begin{aligned} p_{\rm sa} W/t_{\rm sa} &= \epsilon_{\rm sa} \int ds\ \left(|E_{\rm sa\parallel}|^2 + |E_{\rm sa\perp}|^2\right) \\ &= \epsilon_{\rm sa} \int ds\ |E_{\rm a\parallel}|^2 + \epsilon_{\rm sa}^{-1} \textstyle\int ds\ |E_{\rm a\perp}|^2. \end{aligned} \tag{S4}$$

II. SIMULATION APPROACH

The coplanar and microstrip structures were simulated using the electric quasi-statics component of the finite element solver COMSOL's AC/DC module[3]. We simulated a two dimensional cross-section with half of the resonator, using symmetry to account for the other half. We used adaptive meshing as a starting point and then performed additional meshing around the edges and the corners. We treated the 3 nm by 3 nm square at the metal-air-substrate corner separately to give a corner participation ratio p_c.

To determine the participation ratios, we initially treated the interfaces as 3 nm thick dielectrics with dielectric constant $\epsilon = 10$. However, this area approach is computationally expensive since it requires meshing on the nanometer scale over distances of hundreds of microns. As such, we primarily calculated the participation ratios by computing the electric field on all boundary interfaces with the interface dielectrics excluded from the model and then applying Eqs. (S2)-(S4). This is less

[a)] Electronic mail: martinis@physics.ucsb.edu

computationally expensive as there is no thin dielectric layer explicitly included at the interfaces which needs to be carefully meshed. As indicated in Fig. S1 and Table S1, for two different pairs of simulations, $p_{\rm ms}$, $p_{\rm sa}$, and $p_{\rm ma}+p_{\rm c}$ as calculated by these two approaches typically agree to within 15%, although $p_{\rm ma}$ alone differs by a factor of at least two. This means that the total metal-air interface includes an indeterminate significant fraction of the corners.

We also assumed all surfaces were smooth. Simulations indicate that incorporating smooth bumps on the order of the interface thickness increase the participation ratios and thus loss by a factor of order unity. The value of this factor depends on the interface thickness and on the defect density.

In all of the simulations, we assumed the interfaces to be 3 nm thick. This is not unreasonable for chemi- or physi-sorbed contaminants from the air on the surface such as organics, water, or some oxides. Any substrate surfaces with which ion milling or sputtering has occurred can also have ion damage over thicknesses of the order of 3 nm[4,5]. We note that the metal-substrate interface thickness can be less if treated carefully; TiN sputtered on HF-passivated silicon was observed to have an iterface of 1-2 nm[6], and the thickness can be less than 1 nm if the metal is grown epitaxially on a cleaned and heated substrate[7]. In any of these cases with different thickness interfaces, the participation ratios can be rescaled by the new thickness as per Eqs. (S2)-(S4).

III. RESULTS FOR DIFFERENT GEOMETRIES

Numerical results for a variety of coplanar and microstrip resonator geometries are presented in Table S1. We have calculated the participation ratio p_i and loss $p_i \tan\delta$ for a dielectric with thickness 3 nm, dielectric

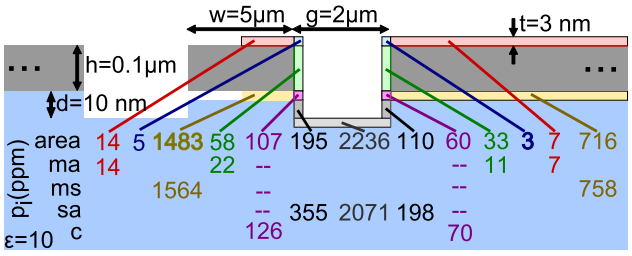

FIG. S1. Etched coplanar waveguide participation ratios. Participation ratios are given in parts per million (ppm) for the metal-air (ma), metal-substrate (ms), and substrate-air (sa) interfaces, as calculated with the surface fields approach with the metal-air-substrate corner (c) treated separately. Participation ratios for the area approach are shown separately. We assumed 3 nm surface dielectrics with $\epsilon_{\rm ma}=\epsilon_{\rm ms}=\epsilon_{\rm sa}=10$; the geometry is given in Table S1 in cases c1 and c2. The participation ratios $p_{\rm ma}+p_{\rm c}$, $p_{\rm ms}$, and $p_{\rm sa}$ agree to within 15%, validating the simulations against numerical errors.

constant $\epsilon=10$, and loss tangent $\tan\delta=0.002$, typical values for metal or silicon oxides[8]. Since the participation ratio is proportional to thickness, these values can easily be scaled for other parameters. Assuming these parameters, the loss from the metal-air interfaces is typically below 10^{-6}. The second quantity in the sum for the metal-air columns arises from the 3 nm by 3 nm corner at the metal/substrate/air interface. As this is a small area, it shows the sensitivity of the loss to this inside corner and indicates the uncertainty in the metal-air prediction.

For coplanar resonators, a significant effect on total loss comes from etching into the substrate within the coplanar gap. This is important because the etching reduces the divergence of the fields at the corner, as shown in Fig. 2 of the main paper, and because the etching reduces the fields parallel to the metal-substrate interface due to the increased distance from the metal traces. Between the pair of cases c1 and c2 and the pair c3 and c4, it is apparent that $p_{\rm ma}$ is reduced by a factor of 2-3. Further deep etching (2 μm, case c6) reduces $p_{\rm ma}$ by an additional factor of 5 and $p_{\rm sa}$ by a factor of 2 while leaving unchanged $p_{\rm ms}$. This change has been experimentally tested for Si substrates[9], where a feature in the loss versus power saturation curve was identified as substrate-air loss. After etching the substrate caused the feature to disappear and resulted in half the loss, which is consistent with the halving of $p_{\rm sa}$ in case c6. This result is consistent with the discussion in the main paper indicating that the substrate-air interface is a dominant loss mechanism.

As experimentally seen by the Delft group[9], different geometries of coplanar resonators result in somewhat different losses. In comparing cases c1 and c2, there is minimal difference between the area and surface models except for some change in $p_{\rm ma}$ from the inside corner, and comparing cases c4 and c5 indicate that these data are similar to previous work from our group[8]. The metal thickness is shown to have little effect in case c7. Case c8 shows that decreasing the width makes the loss increase. However, in case c9, increasing the gap from 2 to 20 μm gave roughly a factor of 3 reduction in all losses.

Sloped sidewalls are also seen to give different losses by comparing cases c11, c4, and c12, where the metal angle θ at the substrate-corner corner (Fig. S2) was varied. All interfaces except the metal-air interface had the greatest loss in case c11, where the sidewall slope was $\theta=45°$, and the least loss in case c12, where the overetched sidewalls had $\theta=135°$. This is expected since the electric field is predicted to scale with the distance r from corners as $r^{-3/7}$ for $\theta=45°$, $r^{-1/3}$ for $\theta=90°$, and $r^{-1/5}$ for $\theta=135°$[10], thus giving the least field divergence, and thus the lowest loss, at the overetched corner. The metal-air interface exhibits the opposite trend, which is consistent with the same argument for the top corner.

Microstrip resonators show significantly higher capacitance per length, which for the same interface energy results in lower loss. In the base case m1, $p_{\rm sa}$ and $p_{\rm ma}+p_{\rm c}$ are both much less than the corresponding values for

TABLE S1. Simulation results for a variety of microwave resonators, obtained from the primary surface-based model [s], the area model [a], and a previous calculation[8]. Coplanar waveguide and microstrip resonator dimensions are as indictated in Fig. S2; the angle θ enclosed by the metal at the metal-substrate-air corner is assumed to be 90° unless otherwise noted. The + sign in the metal-air column data is for a 3 nm by 3 nm area (c) at the intersection of the metal-air (ma), metal-substrate (ms), and substrate-air (sa) interfaces, and represents an entry that could be split among the three interface types. It is placed in the metal-air column since there it gives the greatest proportional uncertainty and because $p_{\mathrm{ma}} + p_{\mathrm{c}}$ and not p_{ma} alone is comparable between the area and surface models. We assume $\epsilon_{\mathrm{s}} = 10$ and surface dielectrics with $\epsilon = 10$, thickness 3 nm, and loss tangent 0.002.

type	dimensions (μm)	capacitance pF/m	metal-air p_{ma} (ppm)	metal-sub. p_{ms} (ppm)	sub.-air p_{sa} (ppm)	loss metal-air $\times 10^6$	loss metal-sub. $\times 10^6$	loss sub.-air $\times 10^6$
coplanar	w, h, g, d							
c1 [a]	5, 0.1, 2, 0.01	162	119+167	2200	2541	0.24+0.33	4.40	5.08
c2 [s]	5, 0.1, 2, 0.01	162	56+196	2322	2624	0.11+0.39	4.64	5.25
c3 [a]	5, 0.1, 2, 0	163	290+387	2234	2286	0.58+0.77	4.47	4.57
c4 [s]	5, 0.1, 2, 0	163	52+662	3065	2011	0.10+1.32	6.13	4.02
c5 [a[8]]	5, 0.1, 2, 0		600		2000	1.2		4.0
c6 [s]	5, 0.1, 2, 2	104	44+6	2690	1032	0.09+0.01	5.38	2.06
c7 [s]	5, 0.025, 2, 0.01	161	55+209	2376	2735	0.11+0.42	4.75	5.47
c8 [s]	2, 0.1, 20, 0.01	68	33+111	1394	1594	0.07+0.22	2.79	3.19
c9 [s]	5, 0.1, 20, 0.01	85	18+60	847	928	0.04+0.12	1.69	1.85
c10 [s]	5, 0.1, 20, 0	85	17+207	1091	764	0.03+0.41	2.18	1.53
c11 [s]	5, 0.1, 20, 0,$\theta = 45°$	169	32+1414	3727	2267	0.06+2.83	7.45	4.53
c12 [s]	5, 0.1, 20, 0,$\theta = 135°$	158	104+695	2841	1963	0.21+1.39	5.68	3.93
microstrip	w, h, s, d							
m1 [s]	20, 0.2, 2, 0.01	985	10+45	3155	526	0.02+0.09	6.31	1.05
m2 [s]	20, 0.2, 0.2, 0.01	8964	7+55	29942	409	0.01+0.11	59.9	0.82
m3 [s]	10, 0.2, 2, 0.01	539	19+82	3301	964	0.04+0.16	6.60	1.93
m4 [s]	20, 0.02, 2, 0.01	983	10+49	3185	557	0.02+0.10	6.37	1.11
m5 [s]	20, 0.2, 2, 0	987	9.3+189	3301	397	0.02+0.38	6.60	0.79
m6 [s]	20, 0.2, 2, 2	914	4.6+1.9	2924	291	0.009+0.004	5.85	0.58
m7 [s]	20, 0.2, 2, -2	1006	1.5+3.2	3192	241	0.003+0.006	6.38	0.48

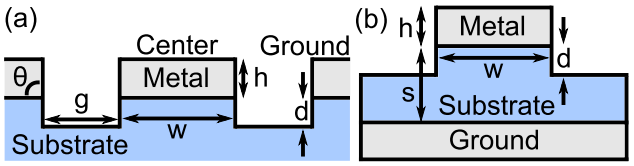

FIG. S2. Coplanar and microstrip dimensions. (**a**) Dimensions for coplanar waveguide simulations. We assume $\theta = 90°$ unless otherwise specified. (**b**) Dimensions for microstrip simulations.

coplanar resonators. However, microstrip resonators also have a larger p_{ms} contribution, approximately equal to the distance ratio $2t/s$ for oxide thickness t. In fact, the thin dielectric of case m2 compared to the base case m1 has a capacitance and p_{ms} approximately 10 times that in case m1 and similar p_{sa} and p_{ma}. Another geometric parameter that is important is the width w, with which p_{ma} and p_{sa} scale inversely, as shown by case m3. However, as indicated in case m4, changing the metal height has minimal effect on the participation ratios.

As with coplanar resonators, changing the depth of etching of the exposed substrate also has a significant effect on loss. The lack of dielectric etching in case m5 results in an increase in p_{ma} from the inside corner of the metal, which is mostly compensated for by a decrease in p_{sa}. Case m6 shows that a deeper etch significantly reduces both of these terms. If, instead of etching the exposed dielectric, the dielectric extends up the sidewall of the metal (as in case m7), the losses are similar to that of a deep etch. Overall, the improvements with etching the exposed dielectric for microstrip resonators are primarily at the metal-air interface, but some effect (factor of 2) is seen for the substrate-air interface. However, the most important concern for a microstrip geometry is a low loss metal-substrate interface, as this loss was dominant in all cases.

IV. DERIVATION OF POWER DEPENDENCE OF PARTICIPATION RATIOS

One potential way to determine which interface dominates the loss is by measuring the power dependence of the loss[9]. When the saturation of surface two-level states (TLSs) at the field E_s is considered, the surface participation ratio p is given by

$$\frac{p}{t\epsilon} = \int_{r_c}^{r_0} \frac{E^2\, dr}{\sqrt{1 + E^2/E_s^2}}, \tag{S5}$$

where the interface has thickness t and dielectric constant ϵ. The electric field is assumed to be dominated by a feature such as a corner with length coordinate r from this feature, characteristic length r_0, and cutoff length $r_c < r_0$.

For a square corner, the field scales[10] as $E = E_0(r/r_0)^{-1/3}$, so substituting this into Eq. (S5) gives a surface participation ratio of

$$\begin{aligned}\frac{p}{t\epsilon} &= E_0^2 \int_{r_c}^{r_0} \frac{(r_0/r)^{2/3}\, dr}{\sqrt{1 + (E_0^2/E_s^2)(r_0/r)^{2/3}}} \\ &= 3E_0^2 r_0 \left[\sqrt{1 + \frac{E_0^2}{E_s^2}} - \sqrt{\left(\frac{r_c}{r_0}\right)^{2/3} + \frac{E_0^2}{E_s^2}} \right]. \end{aligned} \tag{S6}$$

For a thin edge at distances much greater than the film thickness, the field scales[10] as $E = E_0(r/r_0)^{-1/2}$, so substituting this into Eq. (S5) gives a surface participation ratio of

$$\begin{aligned}\frac{p}{t\epsilon} &= E_0^2 \int_{r_c}^{r_0} \frac{(r_0/r)\, dr}{\sqrt{1 + (E_0^2/E_s^2)(r_0/r)}} \\ &= 2E_0^2 r_0 \log \frac{1 + \sqrt{1 + \frac{E_0^2}{E_s^2}}}{\sqrt{\frac{r_c}{r_0}} + \sqrt{\frac{r_c}{r_0} + \frac{E_0^2}{E_s^2}}}. \end{aligned} \tag{S7}$$

[1] J. Koch, T. M. Yu, J. M. Gambetta, A. A. Houck, D. I. Schuster, J. Majer, A. Blais, M. H. Devoret, S. M. Girvin, and R. J. Schoelkopf, Phys. Rev. A **76**, 042319 (2007).

[2] J. Gao, M. Daal, A. Vayonakis, S. Kumar, J. Zmuidzinas, B. Sadoulet, B. A. Mazin, P. K. Day, and H. G. Leduc, Appl. Phys. Lett. **92**, 152505 (2008).

[3] COMSOL 3.6 (COMSOL AB: Stockholm, 2007).

[4] B. Y. Yu, W. C. Lin, Y. Y. Chen, Y. C. Lin, K. T. Wong, and J. J. Shyue, Appl. Surf. Sci. **255** 2490-2493 (2008).

[5] J. W. Park, A. J. Pedraza, and W. R. Allen, Appl. Surf. Sci. **103** 39-48 (1996).

[6] M. R. Vissers, J. Gao, D. S. Wisbey, D. A. Hite, C. C. Tsuei, A. D. Corcoles, M. Steffen, and D. P. Pappas, Appl. Phys. Lett. **97**, 232509 (2010).

[7] D. L. Medlin, K. F. McCarty, R. Q. Hwang, S. E. Guthrie, and M. I. Baskes, Thin Solid Films **299** 110-114 (1997).

[8] H. Wang, M. Hofheinz, J. Wenner, M. Ansmann, R. C. Bialczak, M. Lenander, E. Lucero, M. Neeley, A. D. O'Connell, D. Sank, M. Weides, A. N. Cleland, and J. M. Martinis, Appl. Phys. Lett. **95**, 233508 (2009).

[9] R. Barends, N. Vercruyssen, A. Endo, P. J. de Visser, T. Zijlstra, T. M. Klapwijk, P. Diener, S. J. C. Yates, and J. J. A. Baselmans, Appl. Phys. Lett. **97**, 023508 (2010).

[10] J. D. Jackson, *Classical Electrodynamics* (Wiley, Hoboken, 1999), Ed. 3, Sec. 2.11.